Kuramoto model with coupling through an external medium

David J. Schwab,[1,a)] Gabriel G. Plunk,[2,a)] and Pankaj Mehta[3]
[1]*Department of Molecular Biology and Physics, Princeton University, Princeton, New Jersey 08854, USA*
[2]*Max-Planck-Institut für Plasmaphysik, EURATOM-Assoziation, Wendelsteinstr. 1, 17491 Greifswald, Germany*
[3]*Department of Physics, Boston University, Boston, Massachusetts 02215, USA*

(Received 23 January 2012; accepted 1 November 2012; published online 12 December 2012)

Synchronization of coupled oscillators is often described using the Kuramoto model. Here, we study a generalization of the Kuramoto model where oscillators communicate with each other through an external medium. This generalized model exhibits interesting new phenomena such as bistability between synchronization and incoherence and a qualitatively new form of synchronization where the external medium exhibits small-amplitude oscillations. We conclude by discussing the relationship of the model to other variations of the Kuramoto model including the Kuramoto model with a bimodal frequency distribution and the Millennium bridge problem. © *2012 American Institute of Physics*. [http://dx.doi.org/10.1063/1.4767658]

Oscillatory dynamical units coupled through a shared environment are an increasingly common experimental system, ranging from single-celled organisms communicating through quorum sensing, such as yeast and synthetic bacteria, to semiconductor lasers. Here, we illustrate the differences these systems exhibit compared with the more frequently studied direct coupling setup as well as unearth novel connections to directly coupled systems with, e.g., a bimodal frequency distribution. We construct phase diagrams as a function of cell density and dilution rate of the shared medium, two commonly controlled experimental parameters. Our results, which distinguish the dynamics of the medium from the order parameter, will be of particular use when measurement of the environment is much easier than measurement of the units themselves and their concomitant order parameter.

I. INTRODUCTION

Spontaneous synchronization of coupled oscillators occurs in many biological, physical, and social systems.[1–3] The onset of synchronization is often described using the Kuramoto model,[4,20] where oscillators are directly coupled to each other through their phase differences. However, in many realistic systems, the coupling between oscillators is not direct and instead occurs through a shared external medium. Examples include populations of synthetically engineered bacteria[5] and single-cell eukaryotes communicating through chemical signals,[6] lasers coupled through a central hub,[7] and even pedestrians walking on a bridge.[8,9] In contrast to directly coupled oscillators, such systems have received relatively little attention.[10,11]

In this paper, we present a generalization of the Kuramoto model where oscillators communicate through a common external medium. As in the usual Kuramoto model, each oscillator is described by a time-dependent phase, $\theta_i(t)$, which in the absence of coupling rotates at its natural frequency ω_i. We concentrate on the case when the number of oscillators is large, $N \gg 1$, and the natural frequencies are assumed to be drawn from a prescribed distribution function, $g(\omega)$, with mean frequency ω_0. The oscillators are coupled through an external medium which has an amplitude and phase described by a complex number $Z(t) = R(t)e^{i\Phi(t)}$. The model can be derived from the system introduced in Ref. 11 to study dynamical quorum sensing by considering the weak interaction limit where the amplitude of each individual oscillator's limit cycle remains approximately constant.

The dynamics of the external medium gives rise to interesting new phenomena not seen in directly coupled oscillators. A key dynamical parameter is the (dimensionless) density, ρ, of oscillators in the surrounding medium. We emphasize that this physical density should not be confused with the phase-space density introduced during the analysis in Sec. III. For large densities, $\rho \to \infty$, our model reduces to the usual Kuramoto model. Surprisingly, in the limit $\rho \to 0$, the phase diagram of our model can be mapped to the phase diagram of a Kuramoto model with a bimodal frequency distribution,[12] but with the absence of standing wave solutions that are present in the symmetric bimodal system. At low but non-zero densities, $\rho \ll 1$, the system exhibits bistability between incoherence and synchronization as well as between two different kinds of synchronized states. Additionally, when $\omega_0 = 0$, the dynamics of our model is in one-to-one correspondence with that of the Millennium bridge problem. Thus, the Kuramoto model with coupling through an external medium represents a particularly simple physical model which captures behavior exhibited by a large number of other Kuramoto-like models.

The outline of the paper is as follows. In Sec. II, we define our model and show how it naturally arises from considering the weak-coupling limit of the dynamic quorum sensing model considered in Ref. 11. In Sec. III, we use the Ott-Antonsen *Ansatz* to derive equations for the dynamics of our model for an arbitrary oscillator-frequency distribution.

[a)]D. J. Schwab and G. G. Plunk contributed equally to this work.

Equations (9), (13), and (15) together constitute the model equations studied in-depth throughout the remainder of the text. In Sec. IV, we consider the special case of Lorentzian distribution where it is possible to derive analytic equations for the stability of various phases. In Sec. V, we use these equations and numerical simulations to construct a phase diagram for our model. In Sec. VI, we discuss the relationship of our model to other problems including the Kuramoto model with a bimodal frequency distribution and the Millennium bridge problem. Finally, we discuss the implications of the model and conclude.

II. DERIVATION OF THE MODEL

The Kuramoto model[20] with oscillators coupled through a shared external medium can be derived by considering the weak coupling limit of the model introduced in Ref. 11. The model in Ref. 11 consists of a population of limit-cycle oscillators, z_i, each with a natural frequency ω_j, diffusively coupled to a shared medium, Z. When chemicals leave the oscillators and enter the medium, they are diluted by a factor $\alpha = V_{int}/V_{ext} \ll 1$, the ratio of the volume of the entire system to that of an individual oscillator. Furthermore, the external media is degraded at a rate J. The dynamics of the system are captured by the equation

$$\frac{dz_j}{dt} = (\lambda_0 + i\omega_j - |z_j|^2)z_j - D(z_j - Z), \tag{1}$$

$$\frac{dZ}{dt} = \alpha D\sum_j (z_j - Z) - JZ, \tag{2}$$

with ω_j drawn from a distribution $h(\omega)$, which we assume to be an even function about a mean frequency ω_0. By introducing a dimensionless density, $\rho = \alpha N$, and shifting to a frame rotating with frequency ω_0, we can rewrite Eq. (2) above as

$$\frac{dZ}{dt} = \frac{\rho D}{N}\sum_j (z_j - Z) - (J + i\omega_0)Z, \tag{3}$$

where the frequencies ω_j are now drawn from a distribution $g(\omega)$ with mean zero.

We are interested in the limit $\lambda_0 \gg D$ where individual oscillators are weakly coupled. In this limit, the amplitude of the limit cycle is not affected by the coupling, and the dynamics is well-described by modeling each oscillator with a single phase variable.[14,20] Explicitly, rewriting Eq. (1) in polar coordinates with $z_i = r_i e^{i\theta_i}$ and $Z = Re^{i\Phi}$ yields

$$\frac{dr_j}{dt} = (\lambda_0 - D - r_j^2)r_j + DR\cos(\Phi - \theta_j), \tag{4}$$

$$\frac{d\theta_j}{dt} = \omega_j + \frac{DR}{r_j}\sin(\Phi - \theta_j). \tag{5}$$

In the large λ_0 limit, the first term dominates the right-hand side of Eq. (4), and thus $r_i \simeq \lambda_0^{1/2}$ in steady-state. Defining $\tilde{r}_i = r_i/\lambda_0^{1/2} \simeq 1$ and $\tilde{R} = R/\lambda_0^{1/2}$, we are left with the reduced equations that define our model

$$\frac{d\theta_j}{dt} = \omega_j + D\tilde{R}\sin(\Phi - \theta_j), \tag{6}$$

$$\frac{d\tilde{Z}}{dt} = \frac{\rho D}{N}\sum_j (e^{i\theta_j} - \tilde{Z}) - (J + i\omega_0)\tilde{Z}. \tag{7}$$

Note that Eq. (6) appears identical to the Kuramoto model, except with the order parameter replaced by the amplitude of the medium. We will drop the tilde in the remainder of this paper and note that $r = 1$ will correspond to the fully synchronized state.

Finally, it is useful to define the Kuramoto order parameter,

$$\bar{z} = \frac{1}{N}\sum_j e^{i\theta_j}. \tag{8}$$

$\bar{z}$ is of order unity when all the oscillators have the same phase and zero when they are completely out of phase. Notice that the external medium communicates with the oscillators only through $\bar{z} = re^{i\phi}$, and we can rewrite Eq. (7) in terms of the order parameter as

$$\frac{dZ}{dt} = \rho D(\bar{z} - Z) - (J + i\omega_0)Z. \tag{9}$$

III. DYNAMICAL EQUATIONS FOR ARBITRARY FREQUENCY DISTRIBUTIONS

A. Thermodynamic limit and the Ott-Antonsen Ansatz

In this section, we derive equations for the time-dependence of the distribution function as well as the steady-state values of the order parameter within the low-dimensional manifold of states introduced by Ott and Antonsen.[13] We have explicitly checked that the dynamics of our model is captured by the Ott-Antonsen *Ansatz* (OAA) using numerical simulations. In what follows, we restrict ourselves to the thermodynamic limit, $N \to \infty$. In this case, the dynamics is well described by the time-dependent density function $f(\theta, \omega, t)$, with the fraction of oscillators of frequency ω lying between θ and $\theta + d\theta$ given by $fd\theta$.

The time evolution of f is governed by the continuity equation

$$\frac{\partial f}{\partial t} + \partial_\theta(f\dot{\theta}) = 0, \tag{10}$$

where dot signifies a derivative with respect to time. Plugging in Eq. (6) and rewriting the result in complex notation gives

$$\frac{\partial f}{\partial t} + \partial_\theta\left[f\omega + \frac{D}{4\pi i}(Ze^{-i\theta} - Z^* e^{i\theta})f\right] = 0. \tag{11}$$

Note that unlike the ordinary Kuramoto model,[4] the external medium, Z, enters in the second term in place of the continuum limit of the usual order parameter, $\bar{z} = \int fe^{i\theta}$. Within the OAA, the dynamics lies on a submanifold where the distribution functions are of the form

$$f(\theta,\omega,t)=\frac{g(\omega)}{2\pi}\left(1+\sum_{n=1}^{\infty}[\alpha^n e^{in\theta}+\text{c.c.}]\right), \tag{12}$$

where $\alpha(\omega,t)$ is a function of ω and t, $g(\omega)$ is the frequency distribution of the oscillator population, and c.c. denotes complex conjugate. Substituting this *Ansatz* into the continuity equation (11) gives

$$\frac{\partial\alpha}{\partial t}+i\omega\alpha+\frac{D}{2}(Z\alpha^2-Z^*)=0. \tag{13}$$

The Ott-Antonsen *Ansatz* can also be used to derive a simple expression for the order parameter $\bar{z}$. In the thermodynamic limit, we can write the order parameter as

$$\bar{z}(t)=\int d\omega d\theta f(\theta,\omega,t)e^{i\theta}. \tag{14}$$

Using Eq. (12) and noting that only the term proportional to $e^{-i\theta}$ is non-zero yields the relation

$$\bar{z}=\int d\omega g(\omega)\alpha^*. \tag{15}$$

We will use this definition extensively in what follows. Equations (9), (13), and (15) together constitute the model equations on the OA manifold and will be extensively studied in the remainder of the paper.

B. Stability of the incoherent state

We start by examining the stability of the incoherent state. The calculation can be done using either the reduced system, Eqs. (9), (13), and (15), or equivalently by starting from Eq. (11) and generalizing the analysis of the original Kuramoto model.[15] In the incoherent state, the phase of the oscillators is uniform and $f=\frac{g(\omega)}{2\pi}$. This corresponds to setting $\alpha(\omega,t)=0$ in Eq. (12) and is clearly a solution to the dynamical equations (9), (13), and (15) when $Z=\bar{z}=0$. To calculate the stability of this state, we linearize the dynamical equations about the incoherent state by taking the asymptotic ordering $\alpha\sim Z\sim\bar{z}\sim\mathcal{O}(\epsilon)$, where $\epsilon\ll 1$. This is equivalent to making the expansion $f=g(\omega)/(2\pi)(1+\epsilon f_1)$, substituting this into Eq. (11) and keeping terms linear in ϵ. One can then multiply the result by $\exp(i\theta)$ and integrate over θ to reduce the system further. On the other hand, comparing the expression $f=g(\omega)/(2\pi)(1+\epsilon f_1)$ with Eq. (12), we can find the relationship $\epsilon f_1=g(\omega)\alpha\exp(i\theta)+c.c.$, and so we can see that f_1 corresponds to $n=\pm1$ terms in the Fourier expansion of f in θ, and we really only need to investigate the dynamics of α. Indeed, we can forgo the analysis of Eq. (11) entirely and simply retain terms linear in α in Eq. (13)

$$\frac{\partial\alpha}{\partial t}+i\omega\alpha-\frac{D}{2}Z^*=0. \tag{16}$$

For stability analysis, it is sufficient to consider exponential solutions of the form $\alpha=A\exp[(\lambda+i\Omega)t]$ and $Z=Z_0\exp[(\lambda-i\Omega)t]$, with λ and Ω real numbers. The parameter λ determines the stability of the incoherent state and Ω is a rotation frequency with $\Omega>0$. In particular, in the co-rotating frame, the steady-state solutions rotate with a frequency $\omega_0-\Omega$, slower than the mean frequency ω_0 due to an external medium-induced "drag." This is in contrast with the usual Kuramoto model with direct coupling where $\Omega=0$. Substituting solutions of this form into Eq. (16) yields

$$A=\frac{DZ_0^*}{2(\lambda+i\Omega+i\omega).} \tag{17}$$

Using this in Eqs. (9) and (15) results in a complex equation for Ω and λ of the form

$$\lambda+i(\omega_0-\Omega)+\rho D+J=\frac{\rho D^2}{2}\int_{-\infty}^{\infty}\frac{d\omega g(\omega)}{\lambda-i(\omega+\Omega)} \tag{18}$$

To determine the boundary of stability, we put $\lambda=0^+$ in the equation above and equate the real and imaginary parts to get

$$\frac{\rho D+J}{\rho D^2}=\pi g(\Omega), \tag{19}$$

$$\frac{\Omega+\omega_0}{\rho D^2}=P\left[\int_{-\infty}^{\infty}d\omega\,\frac{g(\omega)}{\omega+\Omega}\right]. \tag{20}$$

Arriving at this equation, we have used the standard identity $\frac{1}{x+i\epsilon}=P(\frac{1}{x})-i\pi\delta(x)$ when $\epsilon=0^+$, with P denoting principal value. Equation (20) gives implicit equations for the surface in the ρ-D-J parameter space where the incoherent state changes stability. We will use this result to construct the phase diagram for our model.

C. Partially locked solution for arbitrary frequency distribution

For a general frequency distribution $g(\omega)$, we derive an equation governing the partially locked states as follows. For such solutions, we expect that the order parameter and external medium rotate at a constant frequency $-\Omega$ or equivalently $\omega_0-\Omega$ in the co-rotating frame. We look for solutions of the form $\alpha=A(\omega)e^{i\Omega t}, Z=Z_0e^{-i\Omega t}$ and $\bar{z}=\bar{z}_0e^{-i\Omega t}$. Inserting these functional forms into Eq. (13) gives

$$iA(\omega+\Omega)+\frac{D}{2}(Z_0A^2-Z_0^*)=0. \tag{21}$$

Defining $b=\omega+\Omega$ and $R=|Z_0|$, we see that

$$A(b)=\frac{-ib\pm\sqrt{-b^2+D^2R^2}}{DZ_0}. \tag{22}$$

To ensure that the dynamics stays on the Ott-Antonsen manifold, it is necessary to make sure that $|A(\omega)|\leq 1$ for all ω. In particular, this inequality ensures that the sum in Eq. (12) does not diverge. This can be guaranteed by properly choosing the positive or negative solutions to Eq. (22) as follows. Defining

$$A \equiv \chi/DZ_0, \tag{23}$$

it suffices to choose

$$\chi(b) = \begin{cases} -ib + \sqrt{-b^2 + D^2R^2} & -DR < b \\ -ib - \sqrt{-b^2 + D^2R^2} & b < -DR. \end{cases} \tag{24}$$

Finally, we can plug in this *Ansatz* into Eq. (9) to get

$$[i(\omega_0 - \Omega) + \rho D + J]R^2 = DZ_0\rho \int db' g(b' - \Omega)A(b'). \tag{25}$$

Together, Eqs. (23)–(25) give a dispersion relationship between Ω and R for locked solutions.

IV. THE LORENTZIAN DISTRIBUTION

A. Dynamical equations

Equation (25), valid for an arbitrary frequency distribution, must be solved numerically to determine the existence of locked solutions. However, just as in the ordinary Kuramoto model, the mathematics simplifies when $g(\omega)$ is a Lorentzian distribution

$$g(\omega) = \frac{1}{\pi}\frac{\Delta}{\omega^2 + \Delta^2}. \tag{26}$$

For Lorentzians, the integrals over $g(\omega)$ appearing in Eqs. (19), (20), and (25) can be performed explicitly and one is left with algebraic equations. These algebraic equations can then be solved to yield the phase boundary of the incoherent state and the existence of locked solutions parameterized by the frequency and amplitude of the external medium, (Ω, R). One subtlety that remains is that we are not able to analytically determine the stability of locked solutions (except for the incoherent state), and we therefore resort to numerical solutions to test stability.

The incoherence stability boundary can be computed explicitly by substituting Eq. (26) into Eq. (18) and using contour integration. This yields

$$\frac{\Delta\omega_0^2}{\Delta + \rho D + J}\left(1 - \frac{\Delta}{\Delta + \rho D + J}\right) + \Delta(\rho D + J) - \rho D^2/2 = 0. \tag{27}$$

The dynamical equations for locked solutions can also be calculated explicitly for a Lorentzian distribution. The key simplification is that the integral in Eq. (15) can again be performed by contour integration so that

$$\bar{z}(t) = \alpha^*(-i\Delta, t). \tag{28}$$

Thus, evaluating Eq. (13) at $\omega = -i\Delta$, we obtain the following equation for the dynamics of the order parameter

$$\frac{\partial \bar{z}}{\partial t} + \Delta\bar{z} + \frac{D}{2}(Z^*\bar{z}^2 - Z) = 0. \tag{29}$$

Equation (29) and the equation for the external medium Eq. (9) completely specify the dynamics of the system on the Ott-Antonsen manifold.

To look for locked solutions, we substitute the functional form $\bar{z} = re^{i\Omega t}$ into Eq. (9). This implies that

$$Z(t) = \frac{\rho D r}{i(\Omega + \omega_0) + \rho D + J}e^{i\Omega t}. \tag{30}$$

Inserting the solution for $Z(t)$ back into Eq. (29) gives a complex equation for r and the rotation frequency Ω

$$(i\Omega + \Delta)r + \frac{r\rho D^2}{2} \times \left[r^2\frac{1}{\rho D + J - i(\Omega + \omega_0)} - \frac{1}{\rho D + J + i(\Omega + \omega_0)}\right] = 0. \tag{31}$$

Partially locked solutions are solutions to this equation with $r > 0$. Notice that even though the incoherent state, $r = 0$, is always a solution, it can be stable or unstable, and its stability boundary is given by the phase boundary (Eq. (27)).

We now look for other locked solutions, i.e., those with $r > 0$. To do so, we divide Eq. (31) out by r and solve for Ω as a function of $q = r^2$ to get

$$\Omega(q) = -\omega_0 + \rho D\sqrt{\frac{D}{2\Delta}(1 - q) - 1}. \tag{32}$$

Substituting the solution back into Eq. (31) yields a *cubic equation* for $q = r^2$. In general, this expression becomes unwieldy and must be solved numerically. However, we can still draw many conclusions. Physical solutions must have real values of Ω and real, positive values for $q > 0$. Since the end result is a cubic equation for q, there can be 0, 1, 2, or 3 locked solutions for a given parameter range. Each of these solutions can be stable or unstable. We will use these facts to construct a phase diagram in Sec. IV B.

B. Equations in terms of phase difference

It is useful to rewrite the dynamics of our model in terms of the phase difference, ψ, between the order parameter and external medium. Let $Z = Re^{i\Phi}$, $\bar{z} = re^{i\phi}$, and $\psi = \Phi - \phi$. In terms of these variables, we can rewrite the dynamical equations of motion, Eqs. (9) and (29), as

$$\begin{aligned} \dot{r} &= -\Delta r + \frac{D}{2}(1 - r^2)R\cos\psi, \\ \dot{R} &= -(\rho D + J)R + \rho D r\cos\psi, \\ \dot{\psi} &= -\omega_0 - D\frac{R}{2r}\sin\psi(2\rho + r^2 + 1). \end{aligned} \tag{33}$$

These equations fully characterize the dynamics within the Ott-Antonsen manifold.

For the special case of locked solutions, there is a relationship between the phase difference ψ and the rotation frequency Ω. In particular, by examining the phases of Eq. (30), we have

$$\cos\psi = \frac{\rho D + J}{\sqrt{(\rho D + J)^2 + (\Omega + \omega)^2}}. \tag{34}$$

Alternatively, taking the absolute value of Eq. (30) yields a relationship between the magnitude of the order parameter, r, and the amplitude of the oscillations in the external medium, R

$$R = \frac{\rho D}{\sqrt{(\rho D + J)^2 + (\Omega + \omega_0)^2}} r = \frac{\rho D}{\rho D + J} r \cos\psi. \quad (35)$$

Notice that this is consistent with Eq. (33) since $\dot{R} = 0$ for locked solutions.

V. PHASE DIAGRAM AND BISTABILITY

A. Constructing the bifurcation diagram from dynamical equations

In this section, we discuss the bifurcation diagram for our model as determined by Eqs. (27), (31), and (32). The dynamics of the external medium leads to a much richer phase diagram than that for the Kuramoto model with direct coupling. For brevity, we focus our discussion on the case where $g(\omega)$ is a Lorentzian distribution. We have numerically verified that a similar phase diagram occurs for other distributions. Furthermore, to reduce the number of parameters, we concentrate on the case where $\Delta = 0.1$ and $J = 0$. Note that, in contrast to directly coupled oscillators, the solutions exhibit non-trivial Δ dependence because Δ must be compared to the mean frequency ω_0. On the other hand, the behavior for $J \neq 0$ is expected to be qualitatively similar to the $J = 0$ case because the steady-state solutions in Eq. (31) depend on ρ, D, and J only through the two control parameters $\rho D + J$ and ρD^2.

We can use the results from Sec. IV A to derive the phase diagram in the $(\rho - D)$ plane for various values of ω_0 (see Fig. 1). The red line is the incoherence stability boundary given by Eq. (27). The incoherent solution is stable to the left of this line and unstable to the right. Recall that in addition to the incoherent solution, there can exist 0, 1, 2, or 3 locked solutions which can be stable or unstable. These locked solutions are given by the roots of the cubic equation for $q = r^2$ resulting from substituting Eq. (32) into Eq. (31). Furthermore, notice that the only way the number of locked solutions can change is when one of the roots of the corresponding cubic equation changes sign or if new real ones appear. In order for the former to occur, the solution corresponding to the root changing sign should collide with the incoherent solution $r = 0$ and change its stability. Thus, this can occur only at the incoherence boundary given by the red line. This implies that transitions at the incoherence boundary are continuous. On the other hand, new real solutions appear when the discriminant of the corresponding cubic equation equals zero. Note that the phase boundary defined by having zero discriminant is the only place where discontinuous phase transitions can occur. That is, real positive solutions can come into existence here at non-zero amplitude. This occurs, for instance, in the transition from region M1 to B, in the middle panel of Fig. 1. These lines are plotted in blue in the phase diagrams. The number and type of stable equilibria must be identical within each of the regions carved

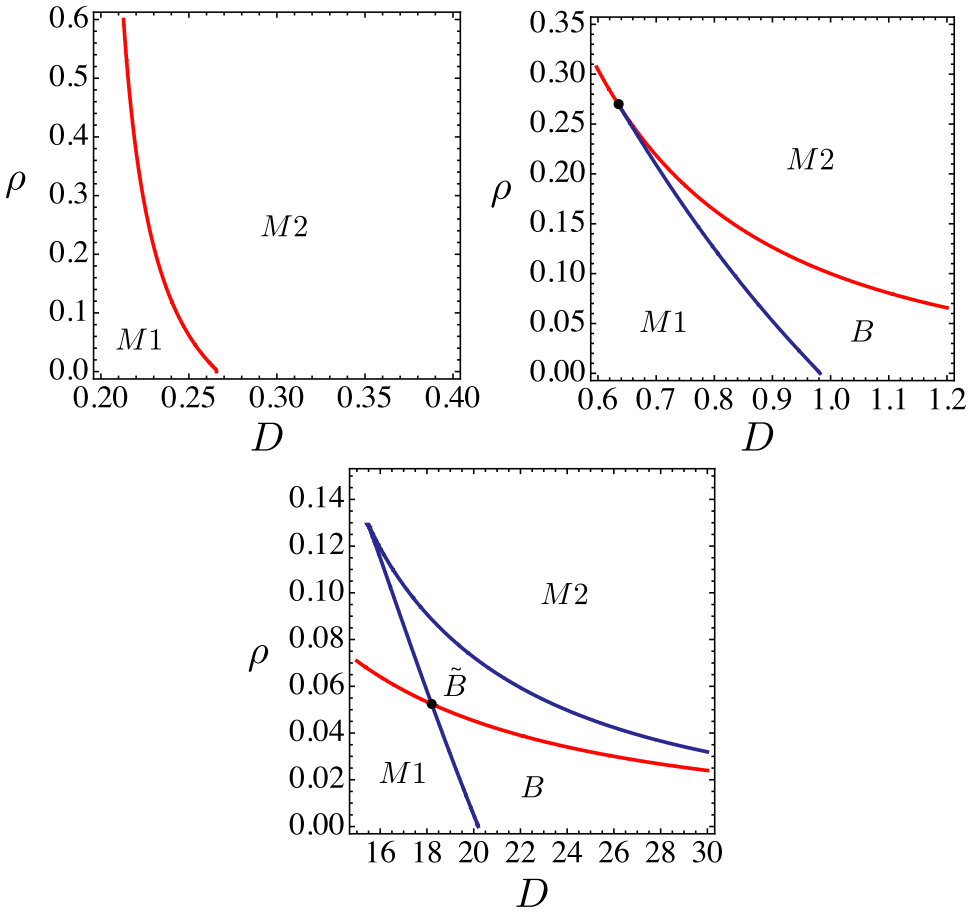

FIG. 1. Phase diagram as a function of parameters. $\Delta = 0.1$ in all figures. (Top) $\omega_0 = 0.0577$, (middle) $\omega_0 = 0.4$, (bottom) $\omega_0 = 10$. M stands for monostability and B stands for bistability. $M1$—incoherence, $M2$—coherent oscillations, B—bistability between incoherent and coherent oscillations, and $\tilde{B}$—bistability between large amplitude phase-locked solution and small amplitude phase-locked solution. Note the change of scale and location of both the horizontal and vertical axes.

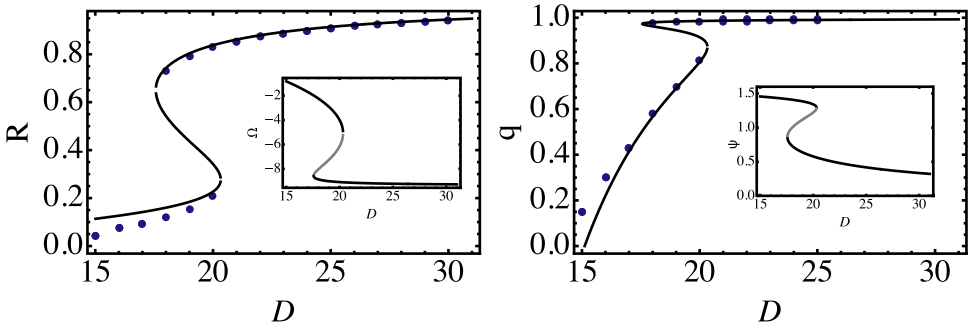

FIG. 2. Amplitude, R, of the external medium (top) and magnitude of the order parameter, r (bottom) for non-trivial locked solutions as a function of coupling D, for $\omega_0 = 10$ and $\Delta = 0.1$. The black lines represent stable solutions and gray lines unstable solutions. Notice the bistable region corresponding to region $\bar{B}$ in Fig. 1. Dots show the result of numerical simulations of $N = 1000$ oscillators. Insets show the locked oscillation frequency in the rotating frame (top) and the phase difference, ψ, between the medium and order parameter, z.

out by the red and blue lines, allowing for a straightforward construction of the phase diagram.

To check these arguments, we ran numerical simulations of $N = 1000$ oscillators with frequencies drawn from a Lorentzian distribution and measured the order parameter after decay of initial transients. We initialized the system with random phases and chose the initial magnitude of R to be either zero or a finite value to probe the stability of the incoherent or partially locked state, respectively. The results were in excellent agreement with the phase diagram in Fig. 1. We also studied a Gaussian $g(\omega)$ distribution and similarly found that the locked solutions exist within the low-dimensional manifold, and the system exhibits qualitatively similar behavior to that found for a Lorentzian distribution.

B. Bifurcation diagram and bistability

We now discuss the bifurcation diagram in greater detail. The top panel in Figure 1 shows a typical bifurcation diagram for small ω_0 and is similar to that for a directly coupled Kuramoto model. There are two phases, an incoherent phase and a locked phase, with a density-dependent critical coupling D that marks the transition between the two phases. As usual, the order parameter r is zero for the incoherent phase and approaches one deep into the partially locked phase.

When ω_0 is increased, as shown in the middle panel of Fig. 1, a bistable region between incoherence and coherence appears at low densities. This region results from the subtle interplay between the "inertia" of the external medium and the amplitude of the order parameter. The influence of the oscillators on the external medium is proportional to the density and the amplitude r of the order parameter, see Eq. (33). Thus, if the oscillators are incoherent, they cannot entrain the media. For large r, the opposite is true, giving rise to the bistable region. At higher densities, the phase diagram is topologically similar to the ordinary Kuramoto model with a direct transition between incoherence and coherence.

The bifurcation diagram develops more features as ω_0 increases further (bottom of Fig. 1). In addition to all of the behaviors discussed above, there also exists a region of bistability between two different locked solutions: one where the amplitude of the external medium oscillations is small and another where the amplitude is large. In both cases, the amplitude of the order parameter r is close to one. The amplitude, R, and the phase difference between the order parameter and external medium, ψ, for these locked solutions can be calculated directly using the aforementioned cubic equation and are shown in Fig. 2. Notice that the external medium oscillates out of phase with the order parameter for the low amplitude locked solution. Finally, we note that the size of this bistable region increases with ω_0.

C. The low amplitude locked solution

A novel consequence of coupling oscillators through an external medium is the existence of the aforementioned locked solution where the order parameter amplitude r is nearly unity but the amplitude of the oscillations in the external medium R is small. Interestingly, this locked solution always appears together with the usual locked solutions where both r and R are close to one. Figure 2 also shows the results of numerical simulations of $N = 1000$ oscillators, confirming the analytic predictions from the Ott-Antonsen *Ansatz*. This new type of locked solution is possible because the effective coupling between oscillators becomes small in Eq. (6) when R is small even when D is large, allowing oscillators to rotate near their natural frequency. Furthermore, Eq. (35) implies that the order parameter and external medium will oscillate at nearly $\pi/2$ out of phase for such a locked state. This can also be seen in the inset of Fig. 2 (bottom).

VI. RELATION TO OTHER SYSTEMS

The model studied here is closely related to other variants of the Kuramoto model. For $\omega_0 = 0$, the steady-state dynamics of our model is identical to that of the Millenium bridge problem.[8,9] Somewhat more surprisingly, in the $\rho \to 0$ limit, the steady-state dynamics of our model can be mapped onto the dynamics of the Kuramoto model with a bimodal frequency distribution[12] (excluding standing wave solutions). We discuss both of these mappings.

A. Millenium bridge problem

To understand wobbly behavior of the Millenium bridge, the authors of Ref. 8 represented the dynamics of pedestrians walking on a bridge using a simple mathematical model in which the bridge is modeled as a driven harmonic

oscillator. Pedestrians are also modeled as oscillators that try to phase lock with the bridge. We now show that the steady-state, locked solutions of the class of systems to which the Millenium bridge belongs can be mapped onto the solutions of our model.

In the Millenium bridge problem, the dynamics of the bridge position, X, is governed by the equation

$$M\frac{d^2X}{dt^2}+B\frac{dX}{dt}+KX=G\sum_{i=1}^{N}\sin\theta_i, \tag{36}$$

with M, B, and K the mass, damping, and stiffness of the bridge, respectively. The "phases" of pedestrian footsteps are represented by the θ_i. It is also useful to write $X=R\sin\Phi$. Notice that for locked solutions where $R=$ cst. and $\Phi=\Omega t$, we can relate the bridge position in the Millenium bridge problem to the external medium in the Kuramoto model by noting that formally we can write $X=\mathrm{Im}\{Z\}$. Furthermore, notice that in the non-rotating, co-rotating frame, isolating the imaginary part of Eq. (2) gives the equation $R\Omega\cos\Phi+(\rho D+J)R\sin\Phi=\frac{\rho D}{N}\sum_j\sin\theta_j$.

Comparison with the equation resulting from substituting a rotating solution $X=R\sin\Phi$ into Eq. (36) yields a mapping between the steady-state dynamics of the two problems. In particular, it is clear that there exists a mapping between parameters $(\rho,D,J,\omega_0)\to(G,B,K,M)$ for which R and Ω are preserved. In particular, assuming $R\neq 0$ gives the mapping $\rho D=\kappa G$, $B=1/\kappa$, and $\rho D+J=\kappa(K-M\Omega^2)$, where $\Omega(\rho,D,J,\omega_0)$ is a function of parameters and $\kappa\neq 0$ is an arbitrary constant. It is interesting that, due to the freedom in specifying κ, the bridge can be under-damped, critically damped, or over-damped.

In the original Millennium bridge problem, the authors restricted their considerations to the case where the natural frequency of the pedestrians and the bridge isidentical.[9] This, they reasoned, is the "worst-case scenario" for wobbling of the bridge. Mathematically, this corresponds to choosing $\omega_0=0$ in the equations above. For this choice, the phase diagram is identical to that of the ordinary Kuramoto model with incoherent and coherent phases (see top of Fig. 1) and this was what was found in Ref. 8. However, as discussed in the last section, the more realistic case where the natural frequency of the pedestrians and bridge differ so that $\omega_0\neq 0$ gives rise to a much richer phase diagram. We also note that the Millennium bridge has been studied[19] with the OA method, but this work only considered the special case $\omega_0=0$.

B. Bimodal distribution

Another variant of the Kuramoto model studied recently using the Ott-Antonsen *Ansatz* is the Kuramoto model with a bimodal frequency distribution. The OA dynamics successfully captures the transition from coherent to incoherent states, including bistability for certain parameters. Within the Ott-Antonsen manifold, it was argued in Ref. 12 that the dynamics of the system is well described by the set of equations for the square of the magnitude of the order parameter $q=r^2$ and a phase difference $\tilde{\psi}$ between the phases of the oscillators locked around $\pm\omega_0$ (see Ref. 12)

$$\dot{q}=-\tilde{\Delta}q+(q-q^2)[\cos\tilde{\psi}+1],\quad \dot{\tilde{\psi}}=\tilde{\omega}_0-(1+q)\sin\tilde{\psi}, \tag{37}$$

where the dot indicates a derivative with respect to $\tilde{t}=D/2t$, $\tilde{\Delta}=(4\Delta)/D$, and $\tilde{\omega_0}=(4\omega_0)/D$.

We now show that the fixed-point steady-state solutions of the model considered in this paper in the limit $\rho\to 0^+$ are identical to those derived from the equations above. To do so, it is useful to work with the dynamical equations (33) in terms of $R=|Z|$, $r=|\bar{z}|$ and the phase difference ψ. Furthermore, we concentrate on the case when $J=0$. Since we are interested in steady-states, we can set $\dot{R}=0$ in Eq. (33) and derive a relationship between R and r given by $R=r\cos\psi$. Substituting this into the remaining two equations gives

$$\begin{aligned}0=\dot{r}&=-\Delta r+\frac{D}{2}(1-r^2)r\cos^2\psi,\\ 0=\dot{\psi}&=-\omega_0-\frac{D}{2}\tan\psi(2\rho+r^2i+1).\end{aligned} \tag{38}$$

Writing $q=r^2$ and taking the limit $\rho\to 0^+$ gives

$$\begin{aligned}0=\dot{q}&=-2\Delta q+Dq(1-q)\cos^2\psi,\\ 0=\dot{\psi}&=-\omega_0-\frac{D}{4}(q+1)\sin 2\psi.\end{aligned} \tag{39}$$

Finally, making the substitution $\tilde{\psi}=2\psi$, $\tilde{t}=D/2t$,˜$=(4\Delta)/D$, and $\tilde{\omega_0}=(4\omega_0)/D$ yields Eq. (37).

The mapping can also be derived by directly examining Eqs. (27) and (31). In the limit $\rho\to 0^+$, the stability boundary of the incoherent state (Eq. (27)) reduces to

$$D=2(\Delta^2+\omega_0^2)/\Delta. \tag{40}$$

This is identical to the corresponding boundary calculated for directly coupled oscillators with a bimodal frequency distribution in Ref. 12. We can also directly derive an equation for the amplitude of frequency-locked solutions in the limit $\rho\to 0^+$ by substituting Eqs. (32) into Eq. (31) and expanding to lowest order in ρ. This procedure yields the equation

$$\omega_0=\pm\frac{1+q}{1-q}\sqrt{\frac{\Delta}{2}(D-Dq-2\Delta)}. \tag{41}$$

As expected, this is identical to the amplitude equation for directly coupled oscillators with a bimodal frequency distribution under the identification $\tilde{\omega}=4\omega/D$, $\tilde{\Delta}=4\Delta/D$. Thus just as in the bimodal case, multiple solutions can arise in our model via a saddle-node bifurcation which occurs when $\partial\omega_0/\partial q=0$ or equivalently $q=2-\frac{\sqrt{D(D+8\Delta)}}{D}$. Substituting this expression into Eq. (41) gives the location of the saddle-node bifurcation with the caveat that when the bifurcation occurs to the left of the incoherence stability boundary, the resulting q is negative and therefore unphysical. By equating this curve with Eq. (41), we find new physical solutions with positive q arise when $\omega_0>\Delta/\sqrt{3}$. We emphasize that this mapping is only valid for fixed-point steady-state solutions

within the OAA. In particular, the system studied in this paper does not inherit the so-called "standing-wave" solutions present in the bimodal case.

Somewhat surprisingly, we have shown that, absent limit cycle solutions (i.e., "standing waves"), the steady-state behavior of our model in the $\rho, J \to 0$ limit is identical, with the same parameters, to that of a Kuramoto model with bimodal distribution restricted to the Ott-Antonsen manifold. This was shown by identifying the phase difference between the order parameter and external medium in our model with twice the phase difference between the order parameters of oscillators locked around $\pm\omega_0$ in the bimodal model. We conclude that the essential physics of both problems is contained in two coupled oscillators.

VII. DISCUSSION

In this paper, we have studied a variation of the Kuramoto model where phase-oscillators are coupled through a common external medium. Such a model is likely to be widely applicable to biological and physical systems where oscillators communicate with each other through some chemical signal or physical membrane. An important distinction between the model studied here and the Kuramoto model is that there is an important new control parameter, the density of oscillators in the medium. This allows for interesting new effects such as a density-dependent transition to oscillations which has been dubbed dynamic quorum sensing.[16,17] We used the Ott-Antonsen *Ansatz* in combination with numerical simulations to investigate the dynamics of this model. We found that the model had a rich phase diagram with bistability between incoherent and locked solutions as well as between two different types of locked solutions. In addition, as summarized in Fig. 3, the model is closely related to other variants of the Kuramoto model in various limits.

The underlying reason for the complex phase diagram in our model is the dynamics of the external medium. The external medium has two distinct effects. First, it introduces an effective time-delay for communication between oscillators. This time-delay manifests itself mathematically by noting that $\Omega \neq 0$. It was previously shown that introducing a fixed time-delay leads to bistability between different locked solutions as is found in this model.[18] However, since the time-delay is not fixed in our model, we do not observe the hierarchy of locked solutions seen in the direct coupling model with delay. Second, the medium has an "inertia" so the natural frequency becomes important. In particular, it is precisely when the natural frequency of the external medium is large that the phase diagram of our model differs the most from the ordinary Kuramoto model.

The steady-state dynamics of the model presented here are equivalent to the Millenium bridge problem when $\omega_0 = 0$. This is unsurprising since the bridge acts as an effective medium through which walkers communicate. What is somewhat unexpected is the richness in the dynamics that emerges when the resonant frequency of the walkers and bridge differs (i.e., $\omega_0 \neq 0$). More surprisingly, the model with an external medium interpolates between a directly coupled Kuramoto model with unimodal and bimodal distributions as a function of the density ρ, with $\rho \to 0$ corresponding to a bimodal distribution, and $\rho \to \infty$ a unimodal distribution (see Fig. 3). An important caveat is that this is only valid for the fixed-point steady-state dynamics of the Kuramoto model with bimodal distribution. The failure of the mapping to capture the standing-wave solutions present in the bimodal case is due to the time-dependence of the order parameter magnitude in such states. It would be interesting to understand the connection between various Kuramoto-like models further through the introduction of "auxiliary" variables such as the external medium studied here.

Perhaps the most experimentally interesting finding of the paper is the predicted bistability regions at low densities. It would be interesting to see if this could be observed in an experimental system. The largest obstacle to this is that in systems where oscillators have both a phase and amplitude, bistability is masked by an oscillator death phase where the amplitude of all oscillators is pulled to zero.[11,21] Thus, any experimental realization would require that the amplitudes of oscillators remain fixed and the phase oscillator approximation apply even at strong couplings. Thus, it is unlikely that bistability exists in experimental setups similar to those used to study dynamical quorum sensing such as the BZ reaction with catalytic beads[17] and quorum-sensing coupled bacteria.[5] Nonetheless, it will be interesting to see if the results here can be experimentally tested.

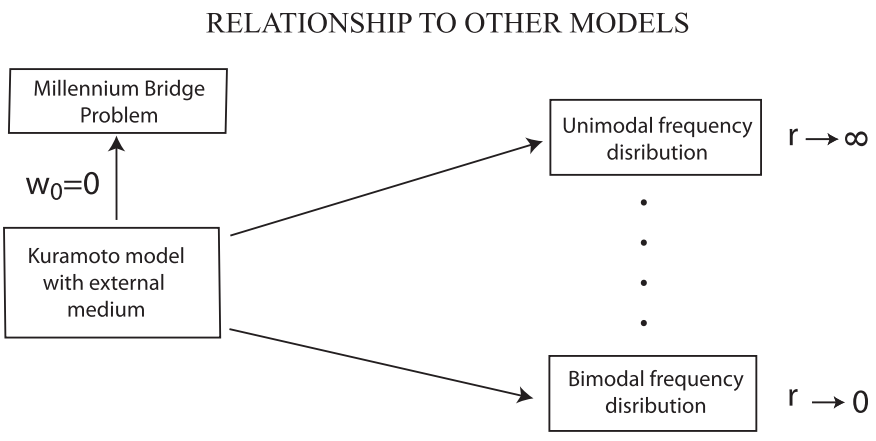

FIG. 3. Relationship of the Kuramoto model with external medium to other variations of the Kuramoto model.

ACKNOWLEDGMENTS

We would like to thank Thomas Antonsen, Thomas Gregor, Troy Mestler, and Javad Noorbakhsh for useful discussions. P.M. and D.S. would like to thank the Aspen Center for Physics where part of this work was performed. D.S. was partially supported by DARPA grant HR0011-18-05-1-0057 and NSF grant PHY-0957573. G.P. was partially supported by DOE Grant No. DESC0005106. P.M. was partially funded by NIH grant K25GM086909.

[1]S. Strogatz, *Sync: The Emerging Science of Spontaneous Order* (Hyperion, 2003).
[2]P. Mehta and T. Gregor, Curr. Opin. Genet. Dev. **20**(6), 574 (2010).
[3]D. Schwab, R. Bruinsma, J. Feldman, and A. Levine, Phys. Rev. E **82**, 051911 (2010).
[4]S. Strogatz, Physica D **143**, 1 (2000).
[5]T. Danino, O. Mondragón-Palomino, L. Tsimring, and J. Hasty, Nature **463**, 326 (2010).
[6]T. Gregor, K. Fujimoto, N. Masaki, and S. Sawai, Sci. STKE **328**, 1021 (2010).
[7]J. Zamora-Munt, C. Masoller, J. Garcia-Ojalvo, and R. Roy, Phys. Rev. Lett. **105**, 264101 (2010).
[8]S. Strogatz, D. Abrams, A. McRobie, B. Eckhardt, and E. Ott, Nature **438**, 3 (2005).
[9]B. Eckhardt, E. Ott, S. Strogatz, D. Abrams, and A. McRobie, Phys. Rev. E **75**, 021110 (2007).
[10]G. Russo and J. Slotine, Phys. Rev. E **82**, 041919 (2010).
[11]D. Schwab, A. Baetica, and P. Mehta, Phys. D **241**(21), 1782 (2012).
[12]E. Martens, E. Barreto, S. Strogatz, E. Ott, P. So, and T. Antonsen, Phys. Rev. E **79**, 026204 (2009).
[13]E. Ott and T. Antonsen, Chaos **19**, 023117 (2009).
[14]Y. Kuramoto, *Chemical Oscillations, Waves, and Turbulence* (Dover, 2003).
[15]P. Matthews, R. Mirollo, and S. Strogatz, Physica D **52**, 293 (1991).
[16]S. De Monte, F. d'Ovidio, S. Danø, and P. Sørensen, Proc. Natl. Acad. Sci. U.S.A. **104**, 18377 (2007).
[17]A. Taylor, M. Tinsley, F. Wang, Z. Huang, and K. Showalter, Science **323**, 614 (2009).
[18]M. Yeung and S. Strogatz, Phys. Rev. Lett. **82**, 648 (1999).
[19]M. Mahmoud and E. Ott, Chaos **19**, 013129 (2009).
[20]J. Acebron, L. Bonilla *et al*., Rev. Mod. Phys. **77**, 137–185 (2005).
[21]R. Mirollo and S. Strogatz, J. Stat. Phys. **60**, 245–262 (1990).